Progress In Electromagnetics Research B, Vol. 90, 109–128, 2021

Radiation from a Dipole Antenna Located outside a Cylindrical Density Depletion in a Magnetoplasma under Resonance Scattering Conditions

Alexander V. Kudrin*, Alexander V. Ivoninsky, and Oleg M. Ostafiychuk

Abstract—Resonance interaction between the electromagnetic radiation from a dipole antenna and a cylindrical density depletion aligned with an external static magnetic field in a magnetoplasma is studied in the case where the antenna is located outside such a density irregularity. A distinctive feature of the presented analysis is using a realistic distribution of the antenna current instead of the assumed one. It is shown that such an antenna can excite plasmon resonances of the density depletion, along with the resonance at the plasma frequency of the outer region. In addition, previously unrevealed resonances of the total field, which are related to excitation of complex modes of the cylindrical density depletion, are discussed. The results obtained can be helpful in understanding the basic properties of resonance interaction of the antenna fields with cylindrical density irregularities in a magnetoplasma and planning the related experiments in the ionospheric and laboratory plasmas.

1. INTRODUCTION

The features of interaction of electromagnetic fields with magnetic-field-aligned plasma density irregularities have been the subject of numerous studies, and there exists a vast literature on various aspects of radiation, propagation, and scattering of waves in the presence of such plasma structures in space and the laboratory [1–17]. An especially strong interest in this problem has been motivated by resonant and guiding properties of a bounded cylindrical plasma in some frequency ranges. Such properties can be used for wave diagnostics of plasma media [18], controlling characteristics of the electromagnetic radiation [19], modification of the wave propagation conditions [20], etc.

The resonance response of an isotropic plasma column in free space to the incidence of a plane electromagnetic wave has since long been known [21, 22], and much work has been done to analyze the corresponding scattering-spectrum maxima known as Tonks-Dattner resonances. These include, in particular, the fundamental quasistatic dipole resonance and weaker temperature-dependent resonances [23–25]. The presence of a static magnetic field superimposed on the plasma column is known to cause significant changes in its resonance response [26–28]. For example, each multipole resonance observed for an isotropic plasma column [23] splits into two resonances under the influence of the external magnetic field [27, 29, 30]. Moreover, additional resonance peaks can be observed near electron cyclotron harmonics in a warm bounded magnetoplasma due to the excitation of Buchsbaum-Hasegawa modes [31, 32]. As a rule, the resonance scattering of the electromagnetic radiation incident from free space on a single axially magnetized plasma column or a set of such columns is characterized by many intriguing behaviors of not only the near- and far-zone fields but also the energy-flow field lines [33–35].

Received 10 November 2020, Accepted 31 December 2020, Scheduled 10 January 2021
* Corresponding author: Alexander V. Kudrin (kud@rf.unn.ru).
The authors are with the Department of Radiophysics, University of Nizhny Novgorod, 23 Gagarin Ave., Nizhny Novgorod 603950, Russia.

Of no less interest is the problem of electromagnetic wave scattering from field-aligned density irregularities located in a magnetoplasma [1, 6, 12]. First of all, this interest is stimulated by the fact that a wide range of plasma density irregularities, which have the transverse dimensions from several meters to a few kilometers, can spontaneously or artificially be created in the ionosphere and the magnetosphere. For example, artificial field-aligned plasma structures are often observed in heating ionospheric [20, 36–44] and laboratory [2–5, 45–48] experiments. Despite significant progress in the studies of scattering characteristics of density irregularities in a magnetoplasma [12–15, 49], little is known about the features of resonance scattering from such plasma structures in the situation where the incident radiation is excited by antennas located near the scattering objects. In this case, the far-field approximation allowing one to replace the incident radiation by a plane wave is no longer applicable, and an exact solution to the problem of scattering of the source-excited electromagnetic waves by the density irregularity is needed. In addition, the possible role of eigenmodes supported by field-aligned plasma density irregularities [17, 19, 47] requires more attention because such modes may be important for understanding some features of resonance scattering.

It should be noted that the problem of excitation of cylindrical plasma structures by given electromagnetic sources has in principle been discussed in the literature. In particular, this problem has been considered in application to determining the excited field in the presence of guiding magnetized plasma structures such as radio-frequency helicon discharges [50–52], magnetic-field-aligned density ducts in space and laboratory plasmas [19, 46, 53–57], and very low-frequency plasma-waveguide antenna systems [58, 59]. However, in all the above-mentioned applications, the electromagnetic sources are usually located inside or on the boundary of a cylindrical plasma object. The case where the electromagnetic source is immersed in the background magnetoplasma surrounding the cylindrical density irregularity has not been considered in sufficient detail, although such a situation may frequently be encountered when dealing with satellite-based antennas. Moreover, the authors are unaware of any major prior study of such a problem for the actual self-consistent distribution of the antenna current driven by an external voltage. Instead, in all works known to us, the current distributions of wire antennas operated in the presence of a cylindrical magnetoplasma are assumed given. However, such an assumption may turn out to be inadequate in some cases requiring knowledge of the realistic current distribution.

It is the purpose of the present work to study the resonance interaction between the field due to a dipole antenna and the cylindrical density depletion embedded in the background magnetoplasma. Assuming that the antenna with a realistic current distribution is located outside the density depletion, the emphasis will be placed on the case where the antenna-current frequency lies in the range containing plasmon resonances of the density depletion.

Our work is organized as follows. In Section 2, we formulate the studied problem. Section 3 presents the general solution for the field excited by a dipole antenna located in the background magnetoplasma parallel to the cylindrical density irregularity. In Section 4, we present numerical results for the characteristics of the excited field under resonance scattering conditions. Our conclusions are summarized in Section 5. Some auxiliary mathematical derivations are given in an appendix.

2. FORMULATION OF THE PROBLEM

We consider an infinitely long, cylindrical density irregularity of radius a in a cold magnetoplasma. It is assumed that this plasma structure is aligned with an external static magnetic field $\mathbf{B}_0$, which is parallel to the z axis of a cylindrical coordinate system (ρ, ϕ, z). The plasma (electron number) density takes the values $\tilde{N} = \text{const}$ and $N = \text{const}$ for $\rho < a$ and $\rho > a$, respectively, such that $\tilde{N} < N$. Choice of density depletion instead of enhancement is driven by the requirement that plasmon resonances of the density irregularity exist in this case [49].

Let the electromagnetic field be excited by a linear dipole antenna located parallel to the density depletion at distance ρ_0 from its axis in the background magnetoplasma, as shown in Fig. 1. The current density of such a source, with $\exp(i\omega t)$ time dependence dropped, is given by

$$\mathbf{J}(\mathbf{r}) = \mathbf{z}_0 I(z)\delta(\mathbf{r}_\perp - \mathbf{r}_{\perp 0})[U(z+L) - U(z-L)], \tag{1}$$

where $I(z)$ is a function describing the distribution of the current along the antenna; L is its half-length; δ is the Dirac function; U is the Heaviside function; $\mathbf{z}_0$ is the unit vector of the z axis; $\mathbf{r}$ is the radius

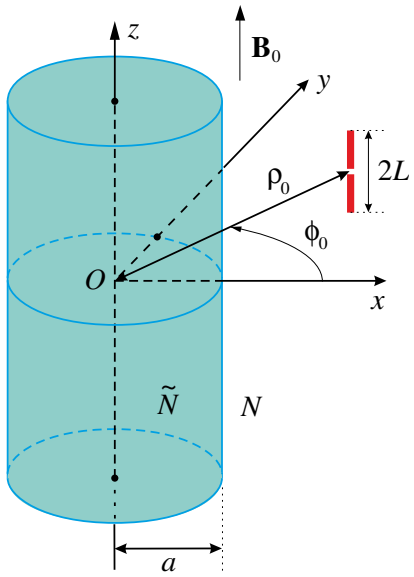

Figure 1. Geometry of the problem.

vector; $\mathbf{r}_\perp$ is its transverse part with respect to $\mathbf{B}_0$; and $\mathbf{r}_{\perp 0}$ is the transverse part of the radius vector specifying the position of the antenna. It is evident that

$$\delta(\mathbf{r}_\perp - \mathbf{r}_{\perp 0}) = \rho^{-1}\delta(\rho - \rho_0)\delta(\phi - \phi_0),$$

where ϕ_0 is the azimuthal coordinate of the antenna.

In the case of a cold magnetoplasma, the complex amplitudes $\mathbf{E}(\mathbf{r})$ and $\mathbf{B}(\mathbf{r})$ of the electromagnetic field excited by the antenna current $\mathbf{J}(\mathbf{r})$ satisfy the Maxwell equations [60, 61]

$$\nabla \times \mathbf{E}(\mathbf{r}) = -i\omega\mathbf{B}(\mathbf{r}), \quad \mu_0^{-1}\nabla \times \mathbf{B}(\mathbf{r}) = i\omega\boldsymbol{\varepsilon} \cdot \mathbf{E}(\mathbf{r}) + \mathbf{J}(\mathbf{r}). \tag{2}$$

Here, μ_0 is the permeability of free space, and $\boldsymbol{\varepsilon}$ is the cold-plasma dielectric tensor which has the form [22, 60]

$$\boldsymbol{\varepsilon} = \epsilon_0 \begin{pmatrix} \varepsilon & -ig & 0 \\ ig & \varepsilon & 0 \\ 0 & 0 & \eta \end{pmatrix}, \tag{3}$$

where ϵ_0 is the permittivity of free space. Recall that the elements of the dielectric tensor in Eq. (3) for a cold magnetoplasma are independent of the wave vector and depend only on the frequency ω and the plasma parameters. This fact allows one to use Eqs. (2) and (3) not only for plane waves but also for the antenna-excited field, which can always be expanded in terms of such waves employing the Fourier transform technique [61].

Assuming that the angular frequency ω of an electromagnetic field is much higher than the lower hybrid resonance frequency, one can write the elements ε, g, and η of the plasma dielectric tensor as [60]

$$\varepsilon = 1 - \frac{\omega_p^2(\omega - i\nu)}{\left[(\omega - i\nu)^2 - \omega_c^2\right]\omega}, \quad g = \frac{\omega_p^2\omega_c}{\left[(\omega - i\nu)^2 - \omega_c^2\right]\omega}, \quad \eta = 1 - \frac{\omega_p^2}{(\omega - i\nu)\omega}, \tag{4}$$

where ω_p and ω_c are the plasma frequency and the cyclotron frequency of electrons, respectively, and ν is the effective electron collision frequency in the plasma. In what follows, we will also assume that the angular frequency is much higher than the electron collision frequency. In the limiting case of a collisionless magnetoplasma, the quantity ε can be represented as $\varepsilon = (\omega^2 - \omega_{\mathrm{UH}}^2)/(\omega^2 - \omega_c^2)$, where $\omega_{\mathrm{UH}} = (\omega_p^2 + \omega_c^2)^{1/2}$ is the upper hybrid resonance frequency.

Throughout this work, we will use the notations ε, g, and η only for the background magnetoplasma ($\rho > a$), while the corresponding quantities for the plasma inside the density depletion ($\rho < a$) will be

denoted as $\tilde{\varepsilon}$, $\tilde{g}$, and $\tilde{\eta}$, respectively. Accordingly, the characteristic frequencies of the magnetoplasma will be denoted as $\omega_{\rm UH}$, ω_p, and ν for $\rho > a$, and as $\tilde{\omega}_{\rm UH}$, $\tilde{\omega}_p$, and $\tilde{\nu}$ for $\rho < a$.

To solve the Maxwell equations (2), we should specify the distribution of the antenna current over the z axis. The current distribution function $I(z)$ of a thin wire antenna is given by antenna theory. For an infinitesimally thin antenna of half-length L excited by the delta-gap voltage generator at $z = 0$, it is known that the function $I(z)$ in the interval $|z| \le L$ is described to a good approximation by the formula

$$I(z) = I_0 \frac{\sin h(L - |z|)}{\sin hL}, \tag{5}$$

where $h = k_0\varepsilon^{1/2}$ is the current distribution constant [62–66]. Here, $k_0 = \omega/c$ is the free-space wave number, with c being the speed of light in free space. The quantity $I_0 = I(0)$ in Eq. (5) is the current at the antenna input. It is important that Eq. (5) for the current distribution of a dipole antenna parallel to $\mathbf{B}_0$ remains valid in all frequency ranges of a magnetoplasma. As is evident from expressions (4), the quantity ε is generally complex-valued such that $\varepsilon = \varepsilon' - i\varepsilon''$. Allowing for the relation $\varepsilon'' \ll |\varepsilon'|$ and assuming that $|h|L\varepsilon''/|\varepsilon'| \ll 1$, which is usually satisfied for reasonable antenna lengths under ionospheric and laboratory conditions, we can put $\varepsilon = \varepsilon'$ when calculating h in Eq. (5).

Since our main interest here is in resonance scattering phenomena that can occur in the response of the cylindrical density depletion to the antenna field, we will focus on the case where plasmon resonances can exist and contribute to the scattered field. Such a depletion is known to have surface plasmon resonances in the frequency interval

$$\tilde{\omega}_{\rm UH} < \omega < \omega_{\rm UH} \tag{6}$$

and volume plasmon resonances at the frequencies below $\tilde{\omega}_{\rm UH}$ [49]. Bearing in mind that the volume plasmon resonances are fairly sufficiently suppressed in the case of even small collision frequencies, we limit ourselves to consideration of the frequency range in Eq. (6). In this range, $\varepsilon' < 0$ and, hence, the quantity h turns out to be imaginary such that $h = -i|h| = -ik_0|\varepsilon'|^{1/2}$ if ε'' is neglected. As a result, Eq. (5) becomes

$$I(z) = I_0 \frac{\sinh |h|(L - |z|)}{\sinh |h|L}. \tag{7}$$

It follows from Eq. (7) that the current distribution takes the "triangular" form $I(z) = I_0(1 - |z|/L)$ for an electrically short antenna when $|h|L \ll 1$. In the opposite case of an electrically long antenna where $|h|L \gg 1$, provided that the condition $|h|L\varepsilon''/|\varepsilon'| \ll 1$ is preserved, the current distribution function reduces to the form $I(z) = I_0 \exp(-|hz|)$, which satisfactorily approximates the current shape along the long dipole antenna, except for the very narrow regions near its ends. This implies that no matter how long the antenna wire might be physically, the current described by Eq. (7) is localized near the antenna input on the length scale of order $|h|^{-1}$ if $|h|L \gg 1$. Because of this fact, one cannot specify the antenna current arbitrarily and should use its distribution predicted by antenna theory.

To avoid misunderstanding, it should also be noted that although the above statements for the antenna current follow from rigorous approaches for the electric dipole in an unbounded magnetoplasma, they remain valid in the presence of a density irregularity unless the distance between the antenna and the depletion boundary becomes of the order of or smaller than the cross-sectional size of the dipole. In the case considered here, this distance is assumed to be much longer, which allows us to use the above-described model for the antenna current.

Thus, the problem becomes one of determining the electromagnetic field due to an electric dipole antenna with the current distribution of Eq. (7) and revealing resonance peaks of the field components as functions of frequency in the presence of a density depletion.

3. SOLUTION FOR THE EXCITED FIELD

To find the electromagnetic field excited by the dipole antenna in the presence of a cylindrical density irregularity, we apply the Fourier transform technique. According to it, any function $f(\mathbf{r})$ and its spatial Fourier transform $f(\mathbf{r}_\perp, p)$ with respect to the z coordinate are related as

$$f(\mathbf{r}) = \frac{k_0}{2\pi} \int_{-\infty}^{\infty} f(\mathbf{r}_\perp, p) \exp(-ik_0 pz) dp,$$

where p has the meaning of the normalized (to k_0) longitudinal wave number.

It can be shown from the Maxwell equations that in the region $\rho > a$, the transverse components $\mathbf{E}_\perp(\mathbf{r}_\perp, p)$ and $\mathbf{B}_\perp(\mathbf{r}_\perp, p)$ of the Fourier-transformed electric and magnetic fields are expressed via the longitudinal components $E_z(\mathbf{r}_\perp, p)$ and $B_z(\mathbf{r}_\perp, p)$ as [19]

$$\mathbf{E}_\perp = \frac{1}{k_0 W}\Big\{ip(\varepsilon - p^2)\nabla_\perp E_z + cg\nabla_\perp B_z + pg(\mathbf{z}_0 \times \nabla_\perp E_z) - ic(\varepsilon - p^2)(\mathbf{z}_0 \times \nabla_\perp B_z)\Big\}, \tag{8}$$

$$\mathbf{B}_\perp = \frac{1}{\omega W}\Big\{-p^2 g\nabla_\perp E_z + icp(\varepsilon - p^2)\nabla_\perp B_z - i\big[g^2 - \varepsilon(\varepsilon - p^2)\big](\mathbf{z}_0 \times \nabla_\perp E_z) + cpg(\mathbf{z}_0 \times \nabla_\perp B_z)\Big\}, \tag{9}$$

where $W = g^2 - (\varepsilon - p^2)^2$ and $\nabla_\perp$ is the transverse (with respect to the z axis) part of the del operator. In turn, the quantities $E_z(\mathbf{r}_\perp, p)$ and $B_z(\mathbf{r}_\perp, p)$ satisfy the following equations in the background magnetoplasma:

$$\nabla_\perp^2 E_z + k_0^2 \frac{\eta}{\varepsilon}(\varepsilon - p^2)E_z + ik_0^2 \frac{g}{\varepsilon} pcB_z = ik_0 \frac{\varepsilon - p^2}{\varepsilon} Z_0 \mathcal{J}(p)\delta(\mathbf{r}_\perp - \mathbf{r}_{\perp 0}), \tag{10}$$

$$\nabla_\perp^2 B_z + k_0^2 \left(\varepsilon - p^2 - \frac{g^2}{\varepsilon}\right) B_z - ik_0^2 \frac{g}{\varepsilon}\eta p c^{-1} E_z = k_0 \frac{g}{\varepsilon} p\mu_0 \mathcal{J}(p)\delta(\mathbf{r}_\perp - \mathbf{r}_{\perp 0}), \tag{11}$$

where

$$\mathcal{J}(p) = \frac{2I_0|h|}{(k_0 p)^2 + |h|^2} \frac{\cosh|h|L - \cos(k_0 pL)}{\sinh|h|L} \tag{12}$$

is the Fourier transform of the function $I(z)$ given by Eq. (7) and $Z_0 = (\mu_0/\epsilon_0)^{1/2}$ is the impedance of free space. Note that the source term (12), which stands on the right-hand sides of Eqs. (10) and (11), does not enter Eqs. (8) and (9) because the antenna current is assumed to have only the z component. It is also worth mentioning that the total field in the outer region $\rho > a$ comprises the field of the dipole antenna in the background magnetoplasma and the scattered field, which is determined by a solution of Eqs. (10) and (11) with zero right-hand sides.

The field in the inner region $\rho < a$ of the density irregularity is described by equations which are obtained from Eqs. (8)–(11) by putting $\mathcal{J} = 0$ and making the replacements

$$\varepsilon \to \tilde{\varepsilon}, \quad g \to \tilde{g}, \quad \eta \to \tilde{\eta}. \tag{13}$$

The desired electromagnetic field should be regular on the z axis as well as satisfy the boundary conditions at $\rho = a$ and the radiation condition at infinity. Note that the boundary conditions consist in continuity of the tangential, i.e., azimuthal and longitudinal, components of the electric and magnetic fields at the surface $\rho = a$, whereas the radiation condition requires that the energy transport, not the phase progress of the waves in the background magnetoplasma, is outgoing at infinity [19].

In the absence of a cylindrical density irregularity, the solution of Eqs. (10) and (11) in a homogeneous plasma with the background parameters can be found as described in Appendix A and has the form

$$\begin{aligned} E_z(\mathbf{r}_\perp, p) &= i\eta^{-1}\sum_{k=1}^{2} C_k n_k q_k H_0^{(2)}(k_0 q_k R_\perp), \\ B_z(\mathbf{r}_\perp, p) &= -c^{-1}\sum_{k=1}^{2} C_k q_k H_0^{(2)}(k_0 q_k R_\perp). \end{aligned} \tag{14}$$

Hereafter, $H_m^{(2)}$ denotes the Hankel function of the second kind of order m and $R_\perp = |\mathbf{r}_\perp - \mathbf{r}_{\perp 0}|$. Other notations in Eq. (14) are defined as

$$\begin{aligned} C_k &= (-1)^k Z_0 \frac{ik_0 pgq_k}{4\varepsilon(q_1^2 - q_2^2)}\mathcal{J}(p), \quad k = 1, 2, \\ n_k &= -\varepsilon\left(q_k^2 + p^2 + \frac{g^2}{\varepsilon} - \varepsilon\right)(pg)^{-1}, \\ q_k &= \Big\{[\varepsilon^2 - g^2 + \varepsilon\eta - (\varepsilon + \eta)p^2 + (-1)^k R(p)]/(2\varepsilon)\Big\}^{1/2}, \end{aligned} \tag{15}$$

where

$$R(p) = \left\{(\varepsilon-\eta)^2 p^4 + 2\left[g^2(\varepsilon+\eta) - \varepsilon(\varepsilon-\eta)^2\right]p^2 + \left(\varepsilon^2 - g^2 - \varepsilon\eta\right)^2\right\}^{1/2}. \tag{16}$$

It may be noted that q_1 and q_2 are the normalized (to k_0) transverse wave numbers corresponding to two normal waves (ordinary and extraordinary) of a magnetoplasma. The branches of the quantities q_1 and q_2 as functions of p are chosen so as to satisfy the inequality $\operatorname{Im} q_k < 0$, at least in the limit of vanishing losses in the plasma, which ensures the fulfillment of the radiation condition at infinity. For definiteness, the function $R(p)$ in Eq. (16) is defined in this case so that $\operatorname{Re}[R(p)] > 0$.

The longitudinal components of the antenna field in the absence of a density irregularity are obtained from their Fourier transforms (14) as follows:

$$\begin{bmatrix} E_z(\mathbf{r}) \\ B_z(\mathbf{r}) \end{bmatrix} = \frac{k_0}{2\pi}\int_{-\infty}^{\infty} \begin{bmatrix} E_z(\mathbf{r}_\perp, p) \\ B_z(\mathbf{r}_\perp, p) \end{bmatrix} \exp(-ik_0 pz)\,dp. \tag{17}$$

The transverse components of the antenna field are obtained from $\mathbf{E}_\perp(\mathbf{r}_\perp, p)$ and $\mathbf{B}_\perp(\mathbf{r}_\perp, p)$ in a similar way. As is known [61], the integral field representation in the form of Eq. (17) yields the exact solution for the total antenna field, including its radiative and reactive parts. The radiative part is given by integration over the intervals of p for which the transverse wave numbers q_k are real. Integration over the remaining intervals of p gives the evanescent-wave and reactive contributions to the field of the antenna.

To facilitate the further analysis, it is convenient to represent the field in the cylindrical coordinate system whose axis coincides with the irregularity axis. Such a representation for the Fourier transforms $E_z(\mathbf{r}_\perp, p)$ and $B_z(\mathbf{r}_\perp, p)$ of the longitudinal field components takes the form

$$\begin{bmatrix} E_z(\mathbf{r}_\perp, p) \\ B_z(\mathbf{r}_\perp, p) \end{bmatrix} = \sum_{m=-\infty}^{\infty} \begin{bmatrix} E_{z,m}(\rho, p) \\ B_{z,m}(\rho, p) \end{bmatrix} \exp(-im\phi), \tag{18}$$

where m is the azimuthal index ($m = 1, \pm1, \pm2, \ldots$), and the terms under the summation sign are the azimuthal harmonics of $E_z(\mathbf{r}_\perp, p)$ and $B_z(\mathbf{r}_\perp, p)$. In what follows, the notations $E_{z,m}$ and $B_{z,m}$ will be used only for the azimuthal harmonics corresponding to the total field. In order to avoid confusion, we will use the superscripts (r) and (i) to denote the azimuthal harmonics referring to the antenna field which is outward radiated to the region $\rho > \rho_0$ and the field excited by the antenna in the region $a < \rho_0 < \rho$, respectively. The latter field can be considered incident on the density irregularity. Correspondingly, the superscripts (t) and (s) will be used for the azimuthal harmonics referring to the field transmitted to the inner region of the density irregularity and the field scattered by it to the background magnetoplasma, respectively.

The azimuthal harmonics of the Fourier-transformed antenna field can be obtained from Eq. (14) using Graf's addition theorem for cylindrical functions [67] and are written in the region $\rho > \rho_0$ as follows:

$$\begin{aligned} E_{z,m}^{(r)}(\rho, p) &= i\eta^{-1}\sum_{k=1}^{2} C_{m,k}^{(r)} n_k q_k H_m^{(2)}(k_0 q_k \rho), \\ B_{z,m}^{(r)}(\rho, p) &= -c^{-1}\sum_{k=1}^{2} C_{m,k}^{(r)} q_k H_m^{(2)}(k_0 q_k \rho). \end{aligned} \tag{19}$$

Here, $C_{m,k}^{(r)} = C_k J_m(k_0 q_k \rho_0)\exp(im\phi_0)$, where J_m is the Bessel function of the first kind of order m. The azimuthal harmonics $E_{z,m}^{(i)}(\rho, p)$ and $B_{z,m}^{(i)}(\rho, p)$, which describe the antenna field incident on the density irregularity, are obtained from Eq. (14) in a similar way, but using Graf's addition theorem under the condition $a < \rho < \rho_0$. The result is

$$\begin{aligned} E_{z,m}^{(i)}(\rho, p) &= i\eta^{-1}\sum_{k=1}^{2} C_{m,k}^{(i)} n_k q_k J_m(k_0 q_k \rho), \\ B_{z,m}^{(i)}(\rho, p) &= -c^{-1}\sum_{k=1}^{2} C_{m,k}^{(i)} q_k J_m(k_0 q_k \rho), \end{aligned} \tag{20}$$

where $C_{m,k}^{(i)} = C_k H_m^{(2)}(k_0 q_k \rho_0) \exp(im\phi_0)$.

The azimuthal harmonics describing the Fourier-transformed field transmitted to the inner region $\rho < a$ of the irregularity are given by

$$\begin{aligned} E_{z,m}^{(t)}(\rho, p) &= i\tilde{\eta}^{-1} \sum_{k=1}^{2} A_{m,k} \tilde{n}_k \tilde{q}_k J_m(k_0 \tilde{q}_k \rho), \\ B_{z,m}^{(t)}(\rho, p) &= -c^{-1} \sum_{k=1}^{2} A_{m,k} \tilde{q}_k J_m(k_0 \tilde{q}_k \rho), \end{aligned} \tag{21}$$

where $A_{m,k}$ is the amplitude coefficient corresponding to the indices m and k, and the quantities $\tilde{n}_k$ and $\tilde{q}_k$ are obtained by making the replacements of Eq. (13) in the above expressions (15) for n_k and q_k, respectively. Note that the quantities of Eq. (21) fully determine the total field inside the irregularity irradiated by the incident field in Eq. (20).

The azimuthal harmonics of the Fourier-transformed scattered field in the region $\rho > a$ can be written as

$$\begin{aligned} E_{z,m}^{(s)}(\rho, p) &= i\eta^{-1} \sum_{k=1}^{2} D_{m,k} n_k q_k H_m^{(2)}(k_0 q_k \rho), \\ B_{z,m}^{(s)}(\rho, p) &= -c^{-1} \sum_{k=1}^{2} D_{m,k} q_k H_m^{(2)}(k_0 q_k \rho), \end{aligned} \tag{22}$$

where $D_{m,k}$ is the scattering coefficient for the corresponding indices. Then the azimuthal harmonics of the total field for $\rho > \rho_0$ or $a < \rho < \rho_0$ are given by summing the antenna-field harmonics of Eqs. (19) or (20), respectively, and the scattered-field harmonics of Eq. (22). It is worth noting that the total field in the region $a < \rho < \rho_0$ is then determined by a linear combination of the first-kind Bessel functions $J_m(k_0 q_k \rho)$ and the second-kind Hankel functions $H_m^{(2)}(k_0 q_k \rho)$ which, in turn, can be represented in terms of $J_m(k_0 q_k \rho)$ and the second-kind Bessel functions $Y_m(k_0 q_k \rho)$ if required.

The unknown coefficients $A_{m,k}$ and $D_{m,k}$ in Eqs. (21) and (22) are determined from the conditions of continuity for the azimuthal and longitudinal field components at the surface $\rho = a$:

$$\begin{aligned} E_{\phi,z;m}^{(t)}(a, p) &= E_{\phi,z;m}^{(s)}(a, p) + E_{\phi,z;m}^{(i)}(a, p), \\ B_{\phi,z;m}^{(t)}(a, p) &= B_{\phi,z;m}^{(s)}(a, p) + B_{\phi,z;m}^{(i)}(a, p). \end{aligned} \tag{23}$$

Solving this system of equations with respect to the desired coefficients $A_{m,1}$, $A_{m,2}$, $D_{m,1}$, and $D_{m,2}$, one can obtain them for each m. In the interests of brevity, cumbersome expressions for these coefficients, which ensure the fulfillment of the boundary conditions at $\rho = a$, are not given here. For the same reason, we do not present the radial and azimuthal field components, which can be obtained by substituting the longitudinal field components into Eqs. (8) and (9) with the corresponding tensor elements.

It is to be emphasized that although the results of this section are applicable to density irregularities with both decreased and enhanced plasma density, the forthcoming numerical results will refer to the irregularities with decreased density because of their ability to respond resonantly to the radiation from the antenna in the frequency range of Eq. (6).

4. NUMERICAL RESULTS

To perform numerical calculations of the scattering properties of the cylindrical density depletion, we chose parameters typical of such field-aligned irregularities under ionospheric conditions. It is assumed that the external static magnetic field $B_0 = 0.5\,\mathrm{G}$ and the plasma densities in the inner and outer regions of the cylindrical irregularity amount to $\tilde{N} = 4.5 \times 10^5\,\mathrm{cm}^{-3}$ and $N = 5 \times 10^5\,\mathrm{cm}^{-3}$, respectively. With these values, the plasma has the characteristic frequencies $\omega_c = 8.79 \times 10^6\,\mathrm{s}^{-1}$, $\tilde{\omega}_p = 3.78 \times 10^7\,\mathrm{s}^{-1}$, $\omega_p = 3.99 \times 10^7\,\mathrm{s}^{-1}$, $\tilde{\omega}_{\mathrm{UH}} = 3.88 \times 10^7\,\mathrm{s}^{-1}$, and $\omega_{\mathrm{UH}} = 4.08 \times 10^7\,\mathrm{s}^{-1}$. The effective collision frequencies $\tilde{\nu}$ and ν, which are determined by the contributions of electron-neutral and electron-ion collisions,

are generally not identical. However, for simplicity, we will be considering the identical values of the effective electron collision frequencies inside and outside the density irregularity. Such a simplification is applicable in the case of a sufficiently small relative plasma density drop-off $(N-\tilde{N})/N$ at $\rho = a$. For the numerical results presented below, the collision frequencies have been taken equal to $\tilde{\nu} = \nu = 600\,\mathrm{s}^{-1}$, which is typical of the lower ionosphere with the assumed background plasma parameters.

For all calculations, we used the source parameters $L = 20\,\mathrm{m}$, $\rho_0 = 15\,\mathrm{m}$, and $\phi_0 = 0$, assuming that the radius of the density irregularity satisfies the condition $a \le 10\,\mathrm{m}$.

To reveal the resonance features in the response of the density depletion to the antenna field, we apply the Fourier inversion to the quantities $E^{(s)}_{z,m}(\rho,p)$ and $B^{(s)}_{z,m}(\rho,p)$ and obtain the azimuthal harmonics $E^{(s)}_{z,m}(\rho,z)$ and $B^{(s)}_{z,m}(\rho,z)$ of the longitudinal components of the scattered field:

$$\begin{bmatrix} E^{(s)}_{z,m}(\rho,z) \\ B^{(s)}_{z,m}(\rho,z) \end{bmatrix} = \frac{k_0}{2\pi} \int_{-\infty}^{\infty} \begin{bmatrix} E^{(s)}_{z,m}(\rho,p) \\ B^{(s)}_{z,m}(\rho,p) \end{bmatrix} \exp(-ik_0 pz)\,dp. \tag{24}$$

Since there are a number of parameters, presenting full numerical results for even a few values of each would take up much space. Therefore, we limit ourselves to discussing the behavior of $E^{(s)}_{z,m}(\rho,z)$ and $B^{(s)}_{z,m}(\rho,z)$ for several values of ρ at $z = 0$ and $z = a$, respectively. The nonzero value of z for $B^{(s)}_{z,m}(\rho,z)$ is chosen in view of the fact that $B^{(s)}_{z,m}(\rho,0) = 0$, which is evident from the symmetry of the problem and easily verified straightforwardly. When plotting the frequency dependences of azimuthal harmonics of the electric and magnetic fields, it is convenient to normalize them to $Z_0|I_0|/a$ and $Z_0|I_0|/ca$, respectively, which makes it possible to present these field quantities in dimensionless form. In what follows, we will also normalize all frequencies to ω_c, so that the lower and upper bounds of the frequency range (6) correspond to $\tilde{\omega}_{\mathrm{UH}}/\omega_c = 4.419$ and $\omega_{\mathrm{UH}}/\omega_c = 4.646$. Note that this range contains the quantity $\omega_p/\omega_c = 4.537$.

The behavior of the field quantities $E^{(s)}_{z,m}(\rho,z)$ and $B^{(s)}_{z,m}(\rho,z)$ as functions of ω at the density depletion surface $\rho = a$ for the chosen values of z is illustrated by Fig. 2 for $a = 5\,\mathrm{m}$. The resonance peaks of various heights are well pronounced in Fig. 2 for $|m| \le 3$. The higher-order resonances with $|m| > 3$ are much weaker than those shown in the figure and, therefore, are not depicted here.

It is evident that the peak of $E^{(s)}_{z,m}(\rho,z)$ for $m = 0$ at the frequency $\omega = \omega_p$ is related to the resonance

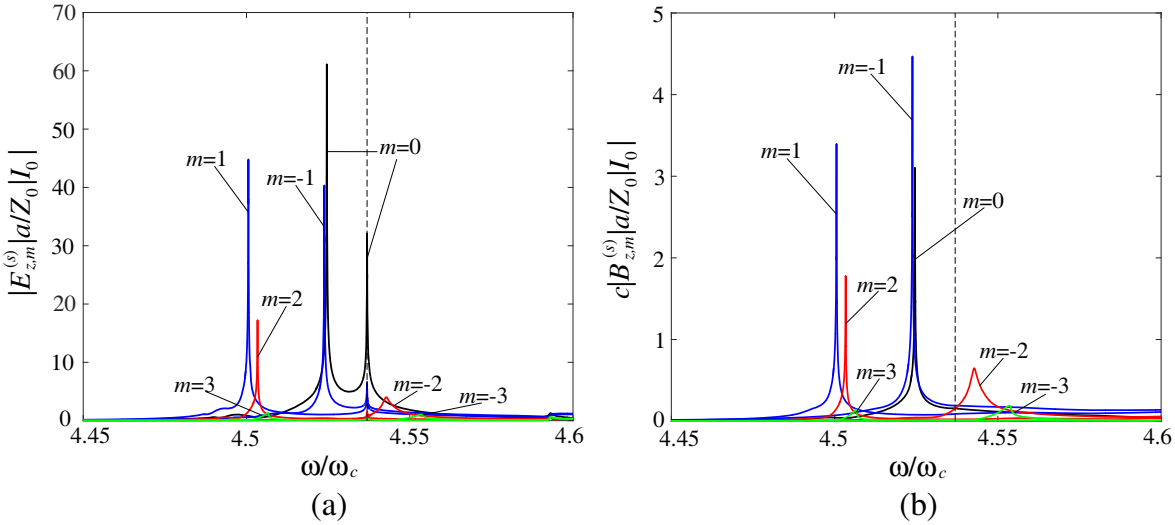

Figure 2. Absolute values of the scattered-field azimuthal harmonics (a) $E^{(s)}_{z,m}(\rho,z)$ and (b) $B^{(s)}_{z,m}(\rho,z)$ at the density depletion surface $\rho = a$ as functions of frequency for $z = 0$ and $z = a$, respectively, in the case where $a = 5\,\mathrm{m}$, $\tilde{N} = 4.5 \times 10^5\,\mathrm{cm}^{-3}$, $N = 5 \times 10^5\,\mathrm{cm}^{-3}$, and $B_0 = 0.5\,\mathrm{G}$. The dashed line shows the position of the plasma frequency ω_p normalized to ω_c.

interaction of the longitudinal electric field with the electrons of the background plasma. Such a peak is expectedly absent in the frequency dependence of $B^{(s)}_{z,m}(\rho, z)$ for $m = 0$. At the same time, four high-Q resonances with the indices $m = 0$, $m = \pm 1$, and $m = 2$ are observed simultaneously for $E^{(s)}_{z,m}(\rho, z)$ and $B^{(s)}_{z,m}(\rho, z)$ at the frequencies $\omega < \omega_p$ in Fig. 2. These peaks, in contrast to other resonances in Fig. 2, cannot be attributed to surface plasmons of a density depletion [49]. This is especially clear for the resonance with $m = 0$ below the plasma frequency ω_p, since no $m = 0$ surface plasmon resonance can exist in the response of a cylindrical density irregularity to the incident radiation. Next, these unusual peaks, which are much narrower than those of the surface plasmon resonances with $m = -2$ and $m = \pm 3$, are not at exactly the surface-plasmon resonant frequencies. Calculating the Q-factor of each resonance as the ratio of the resonant frequency to the full width at half-maximum of the resonance line of the squared field magnitude, one can find that the Q-factors of the narrow-peak resonances are about an order of magnitude greater than those of the plasmon resonances. For example, the Q-factors of the $m = -1$ narrow-peak resonance and the $m = -2$ plasmon resonance in Fig. 2(b) amount to 4.5×10^4 and 1.6×10^3, respectively. Moreover, the number of the unusual high-Q resonances at the frequencies $\omega < \omega_p$ even increases with increasing irregularity radius a. This is evidenced by Fig. 3, which was plotted for $a = 10\,\text{m}$. In addition to the above-mentioned high-Q resonances, one can see new unusual resonances with the indices $m = -2$ and $m = \pm 3$ below the plasma frequency ω_p in Fig. 3.

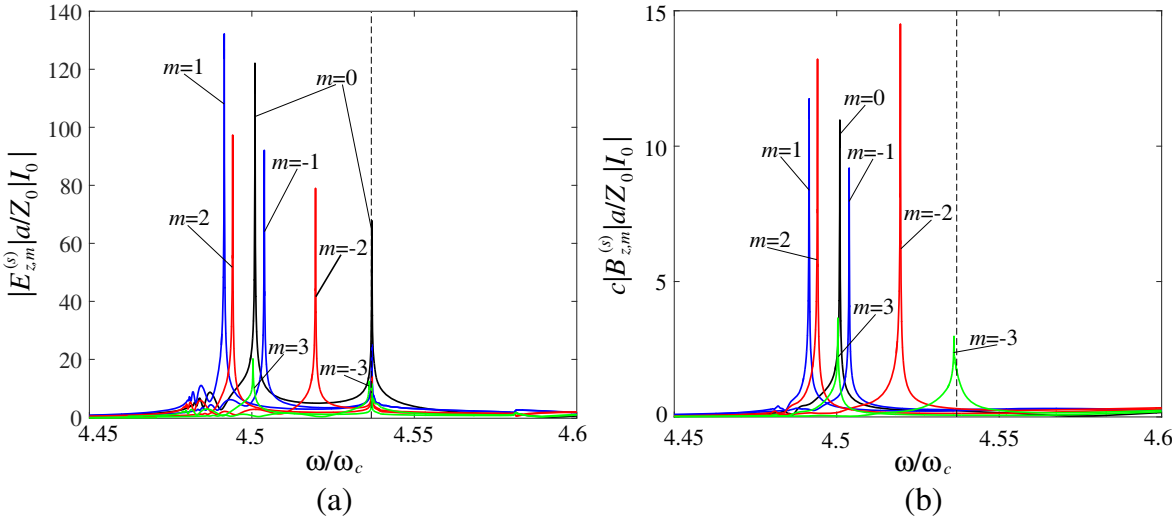

Figure 3. Same as in Fig. 2 but for $a = 10\,\text{m}$.

In order to attempt to clarify what is responsible for appearance for these high-Q resonances, we have analyzed the frequency dependences of the azimuthal harmonics of the field incident on the density depletion. Note that the incident-field harmonics are calculated from their Fourier transforms using a relation that can formally be obtained from Eq. (24) if one replaces the superscript (s) by (i). The frequency dependences of the harmonics $E^{(i)}_{z,m}(\rho, z)$ with the indices $|m| \leq 2$ are shown in Fig. 4. The higher-order harmonics of the incident field are very weak and almost do not affect this field at the surface of the density irregularity. It is seen in Fig. 4 that the azimuthal harmonics of the longitudinal electric-field component are peaked only at the plasma frequency ω_p, which is related to the frequency dependence of the term η^{-1} in the expression for this field component in Eq. (14). Thus, the curves of Fig. 4 do not enable us to explain the appearance of the high-Q resonances below the frequency ω_p in Figs. 2 and 3.

At the same time, we arrive at frequency dependences corresponding to the surface plasmon resonances with increasing distance between the density depletion and the observation point. In this case, the azimuthal harmonics of the scattered field at $\omega > \omega_p$ are much greater in magnitude than those at $\omega < \omega_p$. In view of this, we present the harmonics $E^{(s)}_{z,m}(\rho, z)$ below and above ω_p in separate

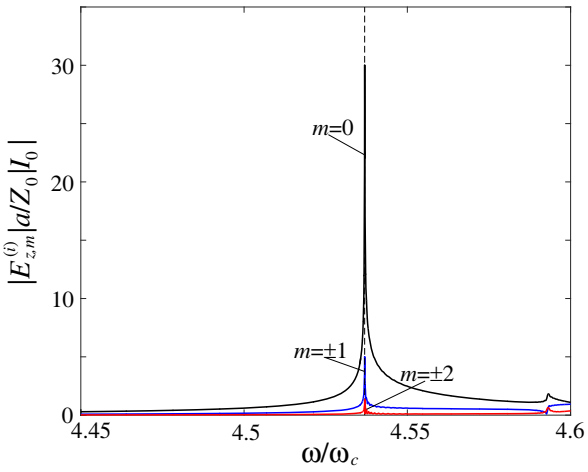

Figure 4. Absolute values of the azimuthal harmonics $E^{(i)}_{z,m}(\rho, z)$ of the incident field at the density depletion surface $\rho = a$ as functions of frequency for $z = 0$, $a = 5\,\mathrm{m}$, and the same plasma parameters as in Fig. 2. The dashed line shows the position of the plasma frequency ω_p normalized to ω_c.

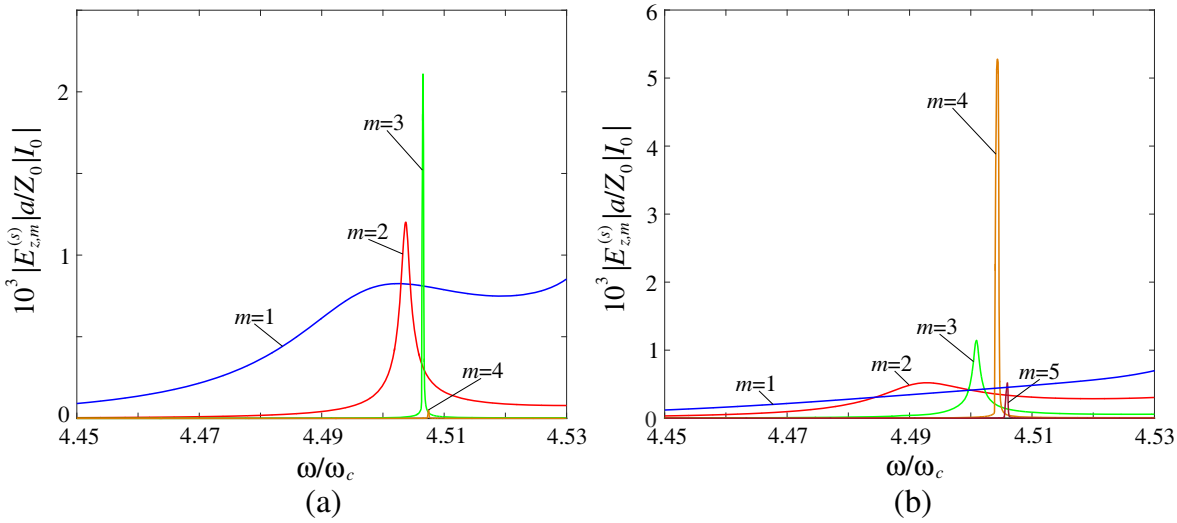

Figure 5. Absolute values of the azimuthal harmonics $E^{(s)}_{z,m}(\rho, z)$ of the scattered field at $z = 0$ and distance $\rho = 50a$ from the density depletion axis as functions of frequency in the range $\tilde{\omega}_{\mathrm{UH}} < \omega < \omega_p$ for (a) $a = 5\,\mathrm{m}$ and (b) $a = 10\,\mathrm{m}$. Same plasma parameters as in Fig. 2.

figures with different scales. The corresponding frequency dependences are shown in Figs. 5 and 6 at $\rho = 50a$ and $z = 0$, in which we excluded the region near the frequency ω_p in order not to show the narrow peak of $E^{(s)}_{z,m}(\rho, z)$ for $m = 0$ at this frequency. We also do not plot the quantities $B^{(s)}_{z,m}(\rho, z)$ at distance $\rho = 50a$ as functions of frequency, because they have the same resonances as in Figs. 5 and 6. It is evident that there are no resonances with $m = 0$ at the frequencies $\omega \neq \omega_p$ in Figs. 5 and 6. The presented resonance curves, especially those in Fig. 5, demonstrate behavior typical of the surface plasmons [49]. This is confirmed by an increase in the radiation loss and, hence, a pronounced smoothing of the resonance curves of the low-m surface plasmons with increasing a. An increase in the resonance-peak heights and then their decrease with increasing $|m|$, which are related in this case to a decrease in the radiation loss of the discussed plasmons and a simultaneous increase in the ohmic-loss influence on them, are also well seen for most curves in these figures. We also observe the notable differences in the shapes of the resonance curves for $\omega < \omega_p$ and $\omega > \omega_p$.

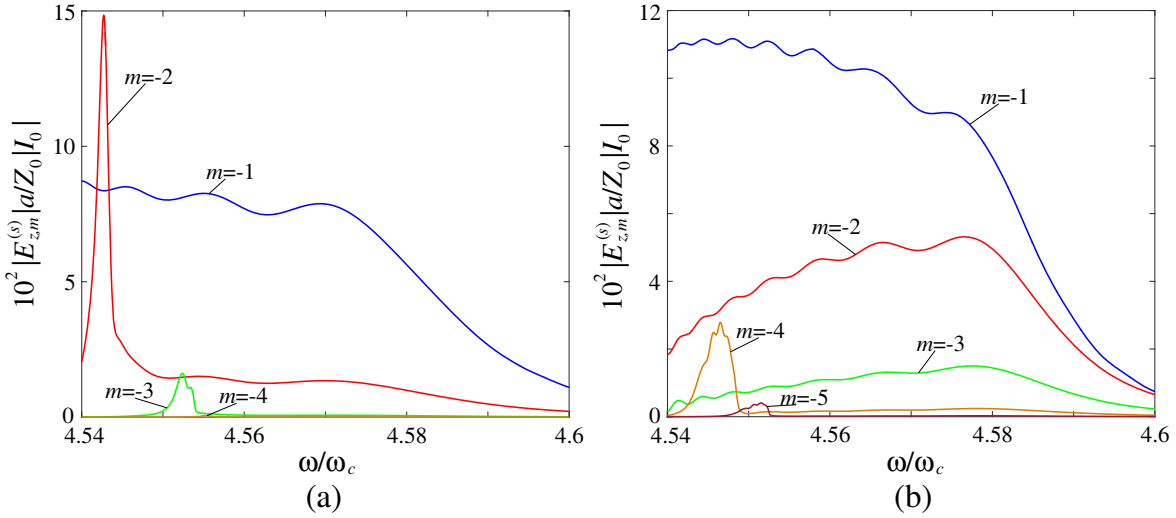

Figure 6. Same as in Fig. 5 but in the range $\omega_p < \omega < \omega_{\mathrm{UH}}$.

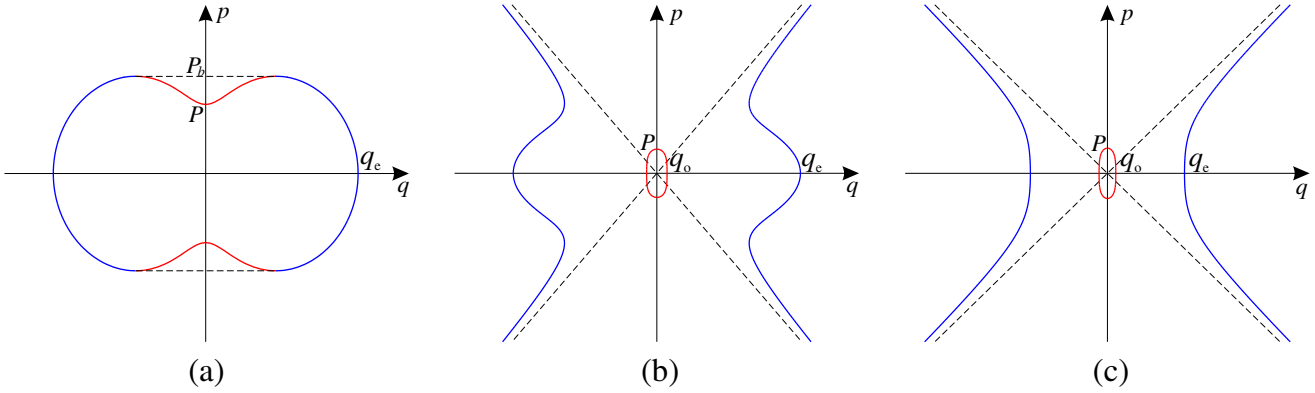

Figure 7. Refractive index surfaces of normal waves in a collisionless magnetoplasma in the frequency ranges (a) $\tilde{\omega}_{\mathrm{UH}} < \omega < \omega_p$, (b) $\omega_p < \omega < \bar{\omega}$, and (c) $\bar{\omega} < \omega < \omega_{\mathrm{UH}}$, which are introduced in Eqs. (25), (26), and (27), respectively.

To explain the results obtained, we now analyze the refractive index surfaces of normal waves of the background magnetoplasma in the frequency interval of Eq. (6) assuming that $\omega_p > \omega_c$, which takes place in the case considered here. The refractive index surfaces at the frequencies in Eq. (6) are shown in Fig. 7. To simplify matters, we present the refractive index surfaces in the case of a collisionless magnetoplasma since allowance for the small collision frequency affects the refractive index of each normal wave only slightly. It is seen in Fig. 7 that the refractive index surfaces have different forms [61] in the following ranges of the frequency interval of Eq. (6):

$$\tilde{\omega}_{\mathrm{UH}} < \omega < \omega_p, \tag{25}$$

$$\omega_p < \omega < \bar{\omega}, \tag{26}$$

$$\bar{\omega} < \omega < \omega_{\mathrm{UH}}, \tag{27}$$

where $\bar{\omega} = [(\omega_p^4 + \omega_c^4/4)^{1/2} + \omega_c^2/2]^{1/2}$. In Fig. 7, $P = (\varepsilon + g)^{1/2}$, $q_{\mathrm{e}} = [(\varepsilon^2 - g^2)/\varepsilon]^{1/2}$, $q_{\mathrm{o}} = \eta^{1/2}$, and the blue and red lines are given by the relations $q^2 = q_1^2(p)$ and $q^2 = q_2^2(p)$, respectively. The quantity $p = P_b$, which is shown in Fig. 7(a), is the root of the equation $R(p) = 0$. The other root $p = P_c$ of this equation is located above P_b on the p axis in the frequency range of Eq. (25) but not shown in Fig. 7(a). The dashed lines in Figs. 7(b) and 7(c) are given by the relation $\varepsilon q^2 + \eta p^2 = 0$, which describes

quasielectrostatic waves corresponding to the unbounded branches of the refractive index surfaces in ranges of Eqs. (26) and (27). Thus, in the frequency range of Eq. (25), the background plasma is transparent only for the extraordinary wave, also known as the Z mode. It is worth mentioning that the extraordinary wave with the refractive index surface shown in Fig. 7(a) continues to be propagating at frequencies that are lower than $\tilde{\omega}_{\mathrm{UH}}$ [61], but such frequencies are not considered in this work. In ranges of Eqs. (26) and (27), the background plasma is also transparent for the ordinary wave.

It is evident that the curves in Fig. 5 are very close to those observed in the case of incidence of the extraordinary plane wave on the density depletion from the background magnetoplasma [49]. This is explained by the fact that the scattered waves in the frequency range of Eq. (25) have a limited spatial spectrum determined by the condition $-P_b < p < P_b$, as well as by a relatively weak dependence of the surface-plasmon resonant frequency on the propagation direction of the incident wave in this range.

The different behaviors of the curves in Fig. 6 are explained by the unbounded spatial spectrum of the extraordinary wave in ranges of Eqs. (26) and (27). Although both normal waves are propagating at these frequencies and contribute to the scattered field, the latter is predominantly determined by the unbounded branches of the refractive index surface of the extraordinary wave. Interference of the quasielectrostatic waves corresponding to these branches is responsible for the oscillatory structure of the frequency dependences in Fig. 6, which are notably wider than those in Fig. 5. Note that the efficient excitation of quasielectrostatic waves by multipoles, which are induced on the scatterer and correspond to surface plasmons, explains much greater values of the scattered field at the frequencies $\omega > \omega_p$ compared with those at the lower frequencies of the range in Eq. (25).

Interestingly, an infinite range of the p values in the frequency intervals of Eqs. (26) and (27) is also responsible for interference phenomena observed as minor maxima or minima in the source field unless the dipole size L becomes so large that the source spectrum in Eq. (12) ceases to depend on L. These minor features of the source field are observed at frequencies somewhat lower than the upper bound in Fig. 4 and can be discerned in Figs. 2(a) and 3(a).

One may pose a question on whether it is possible to ensure narrower surface-plasmon resonances at the frequencies $\omega > \omega_p$, i.e., make them closer to those observed in the case where the density depletion is irradiated by a plane wave [49]. This could evidently be ensured only if the spatial spectrum of waves excited by the source at such frequencies were much narrower than that in the case of a dipole antenna considered here. However, one cannot make this spatial spectrum arbitrarily narrow for an actual antenna. Although the spectrum width decreases with increasing antenna size L, it cannot be narrower than that for $L \to \infty$. But even in this limiting case, the spectrum width is determined by the frequency-dependent scale $|h|^{-1}$ of current decay along the antenna wire and has a finite value which does not allow the resonance curves of the surface plasmons to be narrower than they are at $\omega > \omega_p$ in Fig. 6. This means that use of given sources with arbitrary currents can be inadequate, and consideration of the realistic current distributions given by antenna theory is required.

It remains to explain the origin of the unusual high-Q resonances in Figs. 2 and 3. A careful examination shows that the corresponding resonance peaks exponentially decay and eventually disappear with increasing distance ρ from the density depletion axis. In fact, the high-Q resonances mask the surface plasmon resonances, so that the latter become observable only at sufficiently large distances from the cylindrical density depletion. This circumstance as well as the fact that the high-Q resonances exist only in the frequency range of Eq. (25) allow us to suppose that such resonance features should be related to the excitation of the transversely localized eigenmodes of the depletion at the frequencies $\omega < \omega_p$. Indeed, as is evident from Fig. 7, the density depletion cannot support localized eigenmodes at the frequencies lying in ranges of Eqs. (26) and (27) because for any real longitudinal wave number p there exists at least one real transverse wave number, which does not make it possible to ensure localization of the field across the irregularity in the background plasma. Thus, within the cold-plasma model, the eigenmodes can be expected to exist only in the range of Eq. (25).

It turns out that such eigenmodes supported by the density depletion actually exist and contribute to the field near the cylindrical density depletion in the considered case. Recall that the fields of eigenmodes should be sought in the form coinciding with Eqs. (21) or (22) for $\rho < a$ and $\rho > a$, respectively [19]. With these field representations, the boundary conditions for the tangential field components at $\rho = a$ can be satisfied only for some discrete longitudinal wave numbers, which are the propagation constants of the eigenmodes. Localization of their fields in the transverse direction is

ensured by that the propagation constants of the eigenmodes are greater than P_b in magnitude. Then the quantities q_1 and q_2, which correspond to such propagation constants, are either imaginary for $p > P_c$ or complex such that $q_1 = -q_2^*$ for $P_b < p < P_c$, where the asterisk denotes complex conjugation.

Numerical analysis confirms that in the frequency range of Eq. (25), the density depletion supports propagation of the forward and backward eigenmodes for fixed values of m. As an example, Fig. 8 shows the propagation constants of axisymmetric eigenmodes with $m = 0$ as functions of frequency for two values a_1 and a_2 of the depletion radius, assuming for simplicity that $\tilde{\nu} = \nu = 0$. It is seen in this figure that dispersion curves of the forward eigenmode and the backward eigenmode, which are shown by the lower and upper red lines, respectively, tend to each other with increasing frequency. Eventually, the two curves coalesce at a certain frequency, at which they give rise to two modal solutions known as complex modes [68]. For a density depletion with radius $a = 5\,\mathrm{m}$, this frequency, indicated by the black dot in Fig. 8, is equal to $\omega = 4.524\omega_c$, at which $P_b < p < P_c$. Above this frequency, the propagation constants of the two modes become complex, i.e., $p = \pm p' - ip''$. The quantity p'' as a function of frequency is shown by the blue line in Fig. 8.

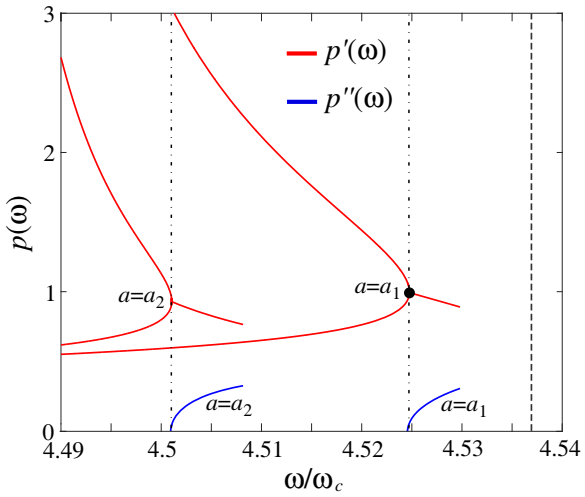

Figure 8. Dispersion curves of eigenmodes of a density depletion for two values of its radius, namely, $a_1 = 5\,\mathrm{m}$ and $a_2 = 10\,\mathrm{m}$, $\tilde{\nu} = \nu = 0$, and the previous values of other plasma parameters. The red and blue curves show the frequency dependences of the real and imaginary parts of the complex propagation constants of modes, respectively. The dashed line denotes the position of the plasma frequency ω_p normalized to ω_c, and the dash-dot lines indicate the frequencies at which the dispersion curves of the forward and backward guided modes coalesce to give rise to the dispersion curves of the complex modes.

As known [68, 69], the complex modes are always excited in pairs, thereby forming the standing-wave resonance structures. The condition for the most efficient excitation of such a wave structure is ensured at the frequency at which the dispersion curves of the forward and backward eigenmodes coalesce. It turns out that all the high-Q resonances in Figs. 2 and 3 are observed exactly at the frequencies at which formation of the complex modes with the indicated indices m occurs from the forward and backward eigenmodes. As far as the authors are aware, this resonance feature was not noted in the previous works dealing with the excitation of such modes by sources located in the outer region of the density depletion. In view of the above, the corresponding peaks in Figs. 2 and 3 may be called the modal resonances. The frequency at which the complex mode appears decreases with increasing radius a. For example, as follows from Fig. 8, this frequency amounts to $\omega = 4.501\omega_c$ when $m = 0$ and $a = 10\,\mathrm{m}$. Such behavior takes place for all m and can be elucidated in the shift of the peaks with variation in a, which is illustrated by the curves for the modal resonances with $|m| \leq 3$ in Fig. 3. Note that the presence of a small collisional loss in the plasma does not affect the above explanation. This loss, however, should be taken into account in the calculations since it determines the Q-factors of the modal resonances.

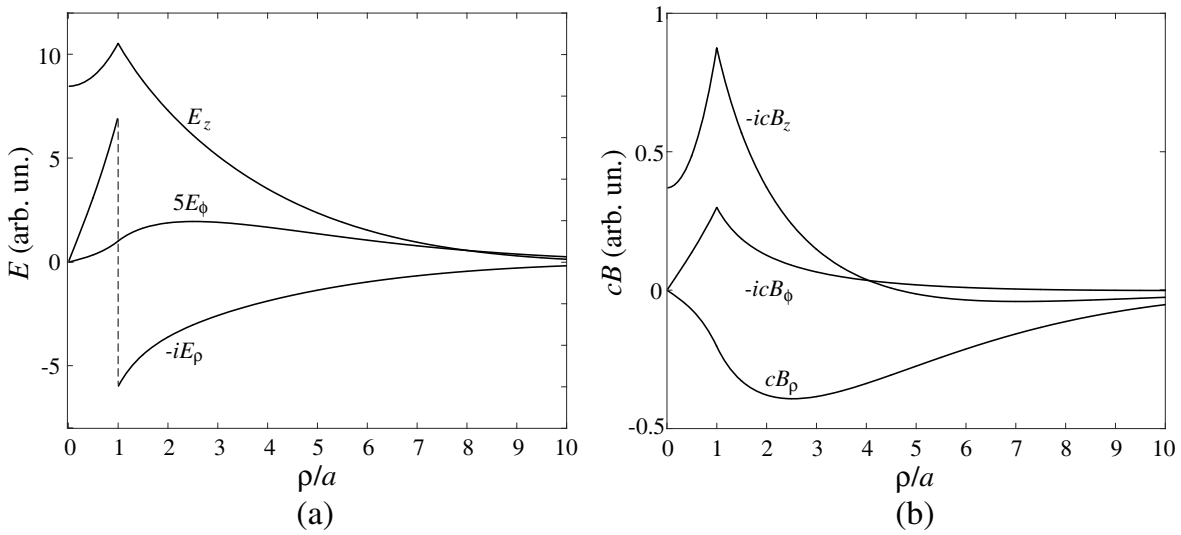

Figure 9. (a) Electric and (b) magnetic components of the eigenmode field as functions of the transverse cylindrical coordinate ρ for a density depletion with radius $a = 5\,\mathrm{m}$ at the frequency $\omega = 4.524\omega_c$ corresponding to the black point in Fig. 8. Other parameters are the same as in Fig. 8.

It is evident that the contribution of modal resonances to the field in the background magnetoplasma decreases with increasing transverse coordinate ρ because complex modes are localized. In particular, the transverse decay length of such modes can amount to a few radii of the density depletion. It is confirmed by Fig. 9 illustrating the modal field structure at a frequency of formation of the $m = 0$ complex modes. Note that the discontinuity of the E_ρ component in Fig. 9 is explained by the used model of a sharp-walled density depletion. It follows from Fig. 9 that there exists another way to suppress the contribution of the modal resonances to the total field. This can be ensured by increasing distance ρ_0 from the source to the density irregularity up to values notably greater than the transverse decay scale of the fields of eigenmodes.

Thus, we can state that different sets of resonances and the related resonance structures of the field can be observed in the near and far zones of the plasma density irregularities. The most interesting field patterns are observed in the case where the antenna frequency ω is rather close to the modal and surface-plasmon resonant frequencies simultaneously. This condition can readily be ensured because all the resonant frequencies are densely located. As an example, Fig. 10 shows snapshots of the E_z component of the total field at $z = 0$ when ω is equal to the almost coinciding frequencies of the $m = 0$ modal resonance and the $m = 3$ surface plasmon resonance of a density depletion with radius $a = 10\,\mathrm{m}$ for the previously used plasma parameters. The presented E_z component is yielded by summing the azimuthal harmonics $E_{z,m}(\rho, z)$ of the total field over m. Since the field absolute values near and far from the depletion are significantly different, the E_z component of the total field cannot be shown on a single plot using the same scale. Therefore, we present the snapshots for $\rho < 4a$ and $\rho > 5a$ on two separate plots. Note that in Fig. 10(a), we do not show the E_z values in the near vicinity of the dipole antenna, where the field is too strong to be presented in the scale adopted for this figure. This region is shown by a white circle in Fig. 10(a). For the same reason, Fig. 10(b) does not show the E_z values in the region $\rho < 5a$, in which the field is much stronger than that at greater values of ρ.

It should be emphasized that the total field in Fig. 10(a) is almost entirely determined by the contribution of the $m = 0$ modal resonance, except for the narrow region near the depletion surface, where the contribution of the $m = 3$ surface plasmon is discernable, and the near-antenna region in which the axisymmetric field structure is perturbed by the field of the dipole antenna. For $\rho > 5a$ [see Fig. 10(b)], the field is already determined by the resonance scattering which corresponds to the $m = 3$ surface plasmon. As a result, the total-field pattern at the chosen frequency demonstrates switch over from one resonance structure to the other with distance from the density depletion. It is evident that allowance for such behavior can be of essential importance if antennas used for diagnosing density

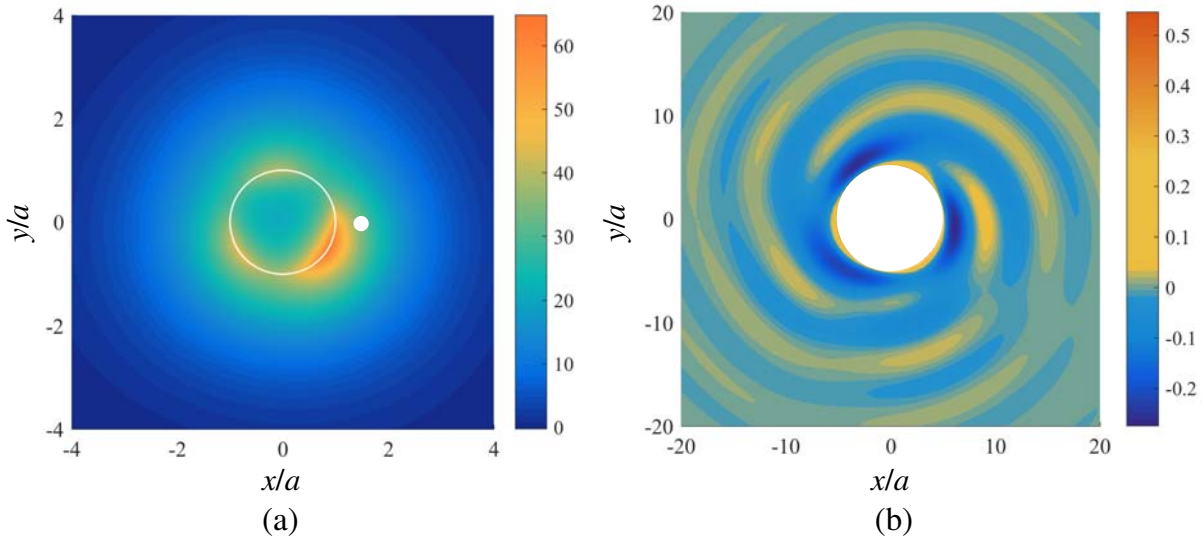

Figure 10. Snapshots of the E_z component of the total field, normalized to $Z_0 I_0/a$, in the regions (a) $\rho < 4a$ and (b) $\rho > 5a$ for $z = 0$ at the frequency $\omega = 4.501\omega_c$, which corresponds to the maxima of the peaks of the $m = 0$ modal resonance and the $m = 3$ surface plasmon resonance for a density depletion with radius $a = 10\,\text{m}$. Same plasma parameters as in Fig. 2.

irregularities are located at moderately small distances from the studied plasma objects with resonance scattering properties.

5. CONCLUSION

In this work, we have studied the scattering of the electric-dipole radiation by a cylindrical density depletion aligned with an external static magnetic field in the magnetoplasma. It is shown that along with the plasmon resonances and the resonance response at the plasma frequency of the outer region of the density irregularity, the modal resonances can be observed in the total field. These resonances, which were not revealed in the previous works, turn out to be most pronounced in the near zone of the density depletion at the frequencies at which its complex modes appear, provided the antenna is located not too far from the depletion. Although the modal resonances may mask the surface plasmon resonances in the near zone of the density irregularity, the resonance features of the field far from the depletion are determined by the contribution of the surface plasmons. It can also be inferred from the reported results that the surface plasmon resonances observed below the plasma frequency of the background medium seem to be of greater diagnostic value as they are much more pronounced compared with those above this frequency.

Another important implication of the performed analysis is that the resonance scattering characteristics of cylindrical plasma objects are rather sensitive to the features of the spatial spectrum of waves excited by an antenna. Therefore, for correct prediction of these characteristics, use of the actual current distribution given by antenna theory is crucial.

Since the resonance phenomena discussed in this work have been shown to exist under conditions typical of the heating experiments in the Earth's ionosphere, the results obtained can be useful in interpreting data of experiments on wave diagnostics of natural and artificial cylindrical density irregularities in the ionospheric plasma. Account of the revealed phenomena can be of essential importance if an antenna used for diagnostic purposes is placed at moderately small distances from the plasma density irregularity. For example, this may be the case where such an antenna is mounted on a miniaturized satellite flying around the density irregularity or on board a spacecraft whose trajectory turns out to be close to such an irregularity. An analogous situation can also be encountered when studying the corresponding effects under conditions of laboratory experiments.

ACKNOWLEDGMENT

This work was supported by the Ministry of Science and Higher Education of the Russian Federation (project No. 0729-2020-0040).

APPENDIX A. DERIVATION OF THE FIELD OF A DIPOLE ANTENNA IN A HOMOGENEOUS MAGNETOPLASMA

We present here the salient steps of the derivation of a solution in Eq. (14) for the Fourier-transformed field components $E_z(\mathbf{r}_\perp, p)$ and $B_z(\mathbf{r}_\perp, p)$ of a dipole antenna in an unbounded homogeneous magnetoplasma.

To obtain this solution, we apply the two-dimensional Fourier transform to the system of Eqs. (10) and (11) with respect to the transverse spatial coordinates. For the Dirac function on the right-hand sides of Eqs. (10) and (11), we then have the representation

$$\delta(\mathbf{r}_\perp - \mathbf{r}_{0\perp}) = \frac{k_0^2}{(2\pi)^2} \int \exp[-ik_0 \mathbf{n}_\perp \cdot (\mathbf{r}_\perp - \mathbf{r}_{\perp 0})] d\mathbf{n}_\perp, \tag{A1}$$

where $\mathbf{n}_\perp = n_x \mathbf{x}_0 + n_y \mathbf{y}_0$ is the orthogonal (to $\mathbf{B}_0$) projection of the wave normals of the plane waves in terms of which functions of the transverse coordinates are expanded by such a Fourier transform. The solution of Eqs. (10) and (11) is sought in a similar form as

$$\begin{bmatrix} E_z(\mathbf{r}_\perp, p) \\ B_z(\mathbf{r}_\perp, p) \end{bmatrix} = \frac{k_0^2}{(2\pi)^2} \int \begin{bmatrix} E_z(\mathbf{n}_\perp, p) \\ B_z(\mathbf{n}_\perp, p) \end{bmatrix} \exp[-ik_0 \mathbf{n}_\perp \cdot (\mathbf{r}_\perp - \mathbf{r}_{\perp 0})] d\mathbf{n}_\perp. \tag{A2}$$

Note that the integration in Eqs. (A1) and (A2) is performed over the entire (n_x, n_y) plane. Substituting representations (A1) and (A2) into Eqs. (10) and (11) yields a system of algebraic equations for $E_z(\mathbf{n}_\perp, p)$ and $B_z(\mathbf{n}_\perp, p)$. Upon solving this system, we obtain

$$\begin{aligned} E_z(\mathbf{n}_\perp, p) &= -\frac{iZ_0 \mathcal{J}(p)}{k_0 D} \left[(\varepsilon - p^2) q^2 - (\varepsilon - p^2)^2 + g^2 \right], \\ B_z(\mathbf{n}_\perp, p) &= -\frac{\mu_0 \mathcal{J}(p)}{k_0 D} pgq^2, \end{aligned} \tag{A3}$$

where $q = |\mathbf{n}_\perp| = (n_x^2 + n_y^2)^{1/2}$ and the quantity D is given by the formula

$$D = \varepsilon q^4 + \left[g^2 - (\varepsilon + \eta)(\varepsilon - p^2) \right] q^2 - \eta \left[g^2 - (\varepsilon - p^2)^2 \right]. \tag{A4}$$

Recall that putting D equal to zero yields the Booker quartic [19], whose solutions $q^2 = q_1^2(p)$ and $q^2 = q_2^2(p)$ are defined in Eq. (15). Hence, Eq. (A4) can be rewritten as

$$D = \varepsilon (q^2 - q_1^2)(q^2 - q_2^2). \tag{A5}$$

We substitute Eq. (A3) into Eq. (A2) and make use of Eq. (A5) along with the decomposition formulas

$$\begin{aligned} \frac{1}{(q^2 - q_1^2)(q^2 - q_2^2)} &= \frac{1}{q_1^2 - q_2^2} \left(\frac{1}{q^2 - q_1^2} - \frac{1}{q^2 - q_2^2} \right), \\ \frac{q^2}{(q^2 - q_1^2)(q^2 - q_2^2)} &= \frac{1}{q_1^2 - q_2^2} \left(\frac{q_1^2}{q^2 - q_1^2} - \frac{q_2^2}{q^2 - q_2^2} \right). \end{aligned}$$

Then it follows that determination of the quantities $E_z(\mathbf{r}_\perp, p)$ and $B_z(\mathbf{r}_\perp, p)$ according to Eq. (A2) is reduced to evaluating the integral

$$\int \frac{\exp\left[-ik_0 \mathbf{n}_\perp \cdot (\mathbf{r}_\perp - \mathbf{r}_{\perp 0})\right]}{q^2 - q_k^2} d\mathbf{n}_\perp = 2\pi \int_0^\infty \frac{q J_0(k_0 q R_\perp)}{q^2 - q_k^2} dq = 2\pi K_0(ik_0 q_k R_\perp), \tag{A6}$$

where K_0 is the modified Bessel function of the second kind of order zero. Note that in deriving Eq. (A6), we passed to new integration variables q and χ in accordance with the relations $n_x = q \cos\chi$

and $n_y = q\sin\chi$. Afterwards, we performed integration over χ from zero to 2π and over q from zero to infinity, using integrals that can be found in tables [67]. It should be emphasized that the integral over q in Eq. (A6) turns out to be convergent under the condition $\mathrm{Im}\, q_k < 0$, which is assumed throughout and ensures the fulfillment of the radiation condition at infinity. Making use of the fact that $K_0(ik_0q_kR_\perp) = -i(\pi/2)H_0^{(2)}(k_0q_kR_\perp)$ [67], we get

$$\begin{aligned} E_z(\mathbf{r}_\perp, p) &= \frac{k_0 Z_0 \mathcal{J}(p)}{4\varepsilon(q_1^2 - q_2^2)} \sum_{k=1}^{2} (-1)^k \left[(\varepsilon - p^2)q_k^2 - (\varepsilon - p^2)^2 + g^2\right] H_0^{(2)}(k_0 q_k R_\perp), \\ B_z(\mathbf{r}_\perp, p) &= -\frac{ik_0\mu_0 p g \mathcal{J}(p)}{4\varepsilon(q_1^2 - q_2^2)} \sum_{k=1}^{2} (-1)^k q_k^2 H_0^{(2)}(k_0 q_k R_\perp). \end{aligned} \tag{A7}$$

Finally, using the notations of Eq. (15) and the identity

$$(\varepsilon - p^2)q_k^2 - (\varepsilon - p^2)^2 + g^2 = -pgn_k q_k^2/\eta,$$

which can be verified by straightforward manipulation, we arrive from Eq. (A7) at the solution of Eq. (14) for the field of a dipole antenna in a homogeneous unbounded magnetoplasma.

REFERENCES

1. Fialer, P. A., "Field-aligned scattering from a heated region of the ionosphere — Observations at HF and VHF," *Radio Sci.*, Vol. 9, No. 11, 923–940, 1974.
2. Stenzel, R. L., "Filamentation instability of a large amplitude whistler wave," *Phys. Fluids*, Vol. 19, No. 6, 865–871, 1976.
3. Sugai, H., M. Maruyama, M. Sato, and S. Takeda, "Whistler wave ducting caused by antenna actions," *Phys. Fluids*, Vol. 21, No. 4, 690–694, 1978.
4. Vdovichenko, I. A., G. A. Markov, V. A. Mironov, and A. M. Sergeev, "Ionizational self-ducting of whistlers in a plasma," *JETP Lett.*, Vol. 44, No. 5, 275–279, 1986.
5. Stenzel, R. L., "Whistler waves in space and laboratory plasmas," *J. Geophys. Res.*, Vol. 104, No. A7, 14379–14395, 1999.
6. Bell, T. F. and H. D. Ngo, "Electrostatic lower hybrid waves excited by electromagnetic whistler mode waves scattering from planar magnetic-field-aligned plasma density irregularities," *J. Geophys. Res.*, Vol. 95, No. A1, 149–172, 1990.
7. Bamber, J. F., W. Gekelman, and J. E. Maggs, "Whistler wave mode conversion to lower hybrid waves at a density striation," *Phys. Rev. Lett.*, Vol. 73, No. 22, 2990–2993, 1994.
8. Calvert, W., "Wave ducting in different wave modes," *J. Geophys. Res.*, Vol. 100, No. A9, 17491–17497, 1995.
9. Streltsov, A. V., M. Lampe, W. Manheimer, G. Ganguli, and G. Joyce, "Whistler propagation in inhomogeneous plasma," *J. Geophys. Res.*, Vol. 111, No. A3, A03216, 2006.
10. Streltsov, A. V., J. Woodroffe, W. Gekelman, and P. Pribyl, "Modeling the propagation of whistler-mode waves in the presence of field-aligned density irregularities," *Phys. Plasmas*, Vol. 19, No. 5, 052104, 2012.
11. Woodroffe, J. R., A. V. Streltsov, A. Vartanyan, and G. M. Milikh, "Whistler propagation in ionospheric density ducts: Simulations and DEMETER observations," *J. Geophys. Res.*, Vol. 118, No. 11, 7011–7018, 2013.
12. Woodroffe, J. R. and A. V. Streltsov, "Whistler interaction with field-aligned density irregularities in the ionosphere: Refraction, diffraction, and interference," *J. Geophys. Res.*, Vol. 119, No. 7, 5790–5799, 2014.
13. Hall, J. O. and T. B. Leyser, "Conversion of trapped upper hybrid oscillations and Z mode at a plasma density irregularity," *Phys. Plasmas*, Vol. 10, No. 6, 2509–2518, 2003.
14. Hall, J. O., Ya. N. Istomin, and T. B. Leyser, "Electromagnetic coupling of localized upper hybrid oscillations in a system of density depletions," *Phys. Plasmas*, Vol. 16, No. 1, 012902, 2009.

15. Eliasson, B. and T. B. Leyser, "Numerical study of upper hybrid to Z-mode leakage during electromagnetic pumping of groups of striations in the ionosphere," *Ann. Geophys.*, Vol. 33, No. 8, 1019–1030, 2015.
16. Starodubtsev, M. V., V. V. Nazarov, M. E. Gushchin, and A. V. Kostrov, "Laboratory modeling of ionospheric heating experiments," *J. Geophys. Res.*, Vol. 121, No. 10, 10481–10495, 2016.
17. Starodubtsev, M., S. Korobkov, M. Gushchin, S. Grach, and V. Nazarov, "Ducting of upper-hybrid waves by density depletions in a magnetoplasma with weak spatial dispersion," *Phys. Plasmas*, Vol. 26, No. 7, 072902, 2019.
18. Benson, R. F., P. A. Webb, J. L. Green, D. L. Carpenter, V. S. Sonwalkar, H. G. James, and B. W. Reinisch, "Active wave experiments in space plasmas: The Z mode," *Lect. Notes Phys.*, Vol. 687, 3–35, 2006.
19. Kondrat'ev, I. G., A. V. Kudrin, and T. M. Zaboronkova, *Electrodynamics of Density Ducts in Magnetized Plasmas*, Gordon and Breach, Amsterdam, 1999.
20. Streltsov, A. V., J.-J. Berthelier, A. A. Chernyshov, V. L. Frolov, F. Honary, M. J. Kosch, R. P. McCoy, E. V. Mishin, and M. T. Rietveld, "Past, present and future of active radio frequency experiments in space," *Space Sci. Rev.*, Vol. 214, 118, 2018.
21. Vandenplas, P. E., *Electron Waves and Resonances in Bounded Plasmas*, Interscience Publishers, London, 1968.
22. Krall, N. A. and A. W. Trivelpiece, *Principles of Plasma Physics*, McGraw-Hill, New York, 1973.
23. Bryant, G. H. and R. N. Franklin, "The scattering of a plane wave by a bounded plasma," *Proc. Phys. Soc.*, Vol. 81, No. 3, 531–543, 1963.
24. Parker, J. V., J. C. Nickel, and R. W. Gould, "Resonance oscillations in a hot nonuniform plasma," *Phys. Fluids*, Vol. 7, No. 9, 1489–1500, 1964.
25. Crawford, F. W., "Internal resonances of a discharge column," *J. Appl. Phys.*, Vol. 35, No. 5, 1365–1369, 1964.
26. Messiaen, A. M. and P. E. Vandenplas, "Resonant behaviour of a cylindrical column of plasma in free space with and without steady magnetic fields," *Physica*, Vol. 28, No. 6, 537–552, 1962.
27. Crawford, F. W., G. S. Kino, and A. B. Cannara, "Dipole resonances of a plasma in a magnetic field," *J. Appl. Phys.*, Vol. 34, No. 11, 3168–3175, 1963.
28. Schmitt, H. J., G. Meltz, and P. J. Freyheit, "Gyrotropic resonances in afterglow plasmas," *Phys. Rev.*, Vol. 139, No. 5A, A1432–A1440, 1965.
29. Seshadri, S. R., "Plane-wave scattering by a magnetoplasma cylinder," *Electron. Lett.*, Vol. 1, No. 9, 256–258, 1965.
30. Vandenplas, P. E. and A. M. Messiaen, "Scattering of electromagnetic waves by a cylindrical plasma in a steady magnetic field: I. Anisotropy effects," *Nucl. Fusion*, Vol. 5, No. 1, 47–55, 1965.
31. Buchsbaum, S. J. and A. Hasegawa, "Excitation of longitudinal plasma oscillations near electron cyclotron harmonics," *Phys. Rev. Lett.*, Vol. 12, No. 25, 685–688, 1964.
32. Buchsbaum, S. J. and A. Hasegawa, "Longitudinal plasma oscillations near electron cyclotron harmonics," *Phys. Rev.*, Vol. 143, No. 1, 303–309, 1966.
33. Es'kin, V. A., A. V. Ivoninsky, and A. V. Kudrin, "Scattering of an obliquely incident plane electromagnetic wave by a magnetized plasma column: Energy flow patterns at plasmon resonances," *Progress In Electromagnetics Research B*, Vol. 63, 173–186, 2015.
34. Es'kin, V. A., A. V. Ivoninsky, A. V. Kudrin, and C. Krafft, "Poynting vector behaviour during the resonance scattering of a plane electromagnetic wave by a gyrotropic cylinder," *Phys. Scr.*, Vol. 91, No. 1, 015502, 2016.
35. Es'kin, V. A., A. V. Ivoninsky, A. V. Kudrin, and L. L. Popova, "Electromagnetic radiation from filamentary sources in the presence of axially magnetized cylindrical plasma scatterers," *J. Exp. Theor. Phys.*, Vol. 124, No. 2, 202–212, 2017.
36. Kelley, M. C., T. L. Arce, J. Salowey, M. Sulzer, W. T. Armstrong, M. Carter, and L. Duncan, "Density depletions at the 10-m scale induced by the Arecibo heater," *J. Geophys. Res.*, Vol. 100, No. A9, 17367–17376, 1995.

37. Stubbe, P., "Review of ionospheric modification experiments at Tromsø," *J. Atmos. Terr. Phys.*, Vol. 58, Nos. 1–4, 349–368, 1996.
38. Frolov, V. L., L. M. Erukhimov, S. A. Metelev, and E. N. Sergeev, "Temporal behaviour of artificial small-scale ionospheric irregularities: Review of experimental results," *J. Atmos. Sol. Terr. Phys.*, Vol. 59, No. 18, 2317–2333, 1997.
39. Tereshchenko, E. D., B. Z. Khudukon, A. V. Gurevich, K. P. Zybin, V. L. Frolov, E. N. Myasnikov, N. V. Muravieva, and H. C. Carlson, "Radio tomography and scintillation studies of ionospheric electron density modification caused by a powerful HF-wave and magnetic zenith effect at mid-latitudes," *Phys. Lett. A*, Vol. 325, Nos. 5–6, 381–388, 2004.
40. Gurevich, A. V., "Nonlinear effects in the ionosphere," *Phys. Usp.*, Vol. 50, No. 11, 1091–1121, 2007.
41. Blagoveshchenskaya, N. F., T. D. Borisova, T. K. Yeoman, M. T. Rietveld, I. M. Ivanova, and L. J. Baddeley, "Artificial small-scale field-aligned irregularities in the high latitude F region of the ionosphere induced by an X-mode HF heater wave," *Geophys. Res. Lett.*, Vol. 38, No. 8, L08802, 2011.
42. Vartanyan, A., G. M. Milikh, E. Mishin, M. Parrot, I. Galkin, B. Reinisch, J. Huba, G. Joyce, and K. Papadopoulos, "Artificial ducts caused by HF heating of the ionosphere by HAARP," *J. Geophys. Res.*, Vol. 117, No. A11, A10307, 2012.
43. Najmi, A., G. Milikh, J. Secan, K. Chiang, M. Psiaki, P. Bernhardt, S. Briczinski, C. Siefring, C. L. Chang, and K. Papadopoulos, "Generation and detection of super small striations by F region HF heating," *J. Geophys. Res.*, Vol. 119, No. 7, 6000–6011, 2014.
44. Grach, S. M., E. N. Sergeev, E. V. Mishin, and A. V. Shindin, "Dynamic properties of ionospheric plasma turbulence driven by high-power high-frequency radiowaves," *Phys. Usp.*, Vol. 59, No. 11, 1091–1128, 2016.
45. Zaboronkova, T. M., A. V. Kostrov, A. V. Kudrin, A. V. Tikhonov, S. V. Tronin, and A. A. Shaikin, "Channeling of waves in the whistler frequency range within nonuniform plasma structures," *Sov. Phys. JETP*, Vol. 75, No. 4, 625–632, 1992.
46. Kostrov, A. V., A. V. Kudrin, L. E. Kurina, G. A. Luchinin, A. A. Shaykin, and T. M. Zaboronkova, "Whistlers in thermally generated ducts with enhanced plasma density: Excitation and propagation," *Phys. Scr.*, Vol. 62, No. 1, 51–65, 2000.
47. Nazarov, V. V., M. V. Starodubtsev, and A. V. Kostrov, "Nonlinear trapping and self-guiding of magnetized Langmuir waves due to thermal plasma filamentation," *Phys. Plasmas*, Vol. 14, No. 12, 122106, 2007.
48. Aidakina, N., M. Gushchin, I. Zudin, S. Korobkov, and A. Strikovskiy, "Laboratory study of interaction of magnetoplasma irregularities produced by several radio-frequency heating sources," *Phys. Plasmas*, Vol. 25, No. 7, 072114, 2018.
49. Ivoninsky, A. V. and A. V. Kudrin, "Resonance scattering of an extraordinary wave by a cylindrical density depletion in a magnetoplasma," *Phys. Plasmas*, Vol. 25, No. 10, 102112, 2018.
50. Arnush, D., "The role of Trivelpiece–Gould waves in antenna coupling to helicon waves," *Phys. Plasmas*, Vol. 7, No. 7, 3042–3050, 2000.
51. Carter, M. D., F. W. Baity, G. C. Barber, R. H. Goulding, Y. Mori, D. O. Sparks, K. F. White, E. F. Jaeger, F. R. Chang-Díaz, and J. P. Squire, "Comparing experiments with modeling for light ion helicon plasma sources," *Phys. Plasmas*, Vol. 9, No. 12, 5097–5110, 2002.
52. Chen, F. F., "Helicon discharges and sources: A review," *Plasma Sources Sci. Technol.*, Vol. 24, No. 1, 014001, 2015.
53. Zaboronkova, T. M., A. V. Kudrin, and M. Yu. Lyakh, "Excitation of nonsymmetric waves by given sources in a magnetoplasma in the presence of a cylindrical plasma channel," *Radiophys. Quantum Electron.*, Vol. 46, Nos. 5–6, 407–424, 2003.
54. Kudrin, A. V., P. V. Bakharev, C. Krafft, and T. M. Zaboronkova, "Whistler wave radiation from a loop antenna located in a cylindrical density depletion," *Phys. Plasmas*, Vol. 16, No. 6, 063502, 2009.

55. Pfannmöller, J. P., C. Lechte, O. Grulke, and T. Klinger, "Investigations on loop antenna excited whistler waves in a cylindrical plasma based on laboratory experiments and simulations," *Phys. Plasmas*, Vol. 19, No. 10, 102113, 2012.
56. Kudrin, A. V., N. M. Shkokova, O. E. Ferencz, and T. M. Zaboronkova, "Whistler wave radiation from a pulsed loop antenna located in a cylindrical duct with enhanced plasma density," *Phys. Plasmas*, Vol. 21, No. 11, 112115, 2014.
57. Kudrin, A. V., O. M. Ostafiychuk, and T. M. Zaboronkova, "Excitation of whistler waves below the lower hybrid frequency by a loop antenna located in an enhanced density duct," *Phys. Plasmas*, Vol. 24, No. 8, 082109, 2017.
58. Kondrat'ev, I. G., A. V. Kudrin, and T. M. Zaboronkova, "The use of near-antenna artificial density ducts for increasing the power of VLF radiation in space plasma," *J. Atmos. Sol. Terr. Phys.*, Vol. 59, No. 18, 2475–2488, 1997.
59. Kudrin, A. V., M. Yu. Lyakh, and T. M. Zaboronkova, "Wave emission from an open-ended cylindrical channel in a cold magnetoplasma," *IEEE Trans. Antennas Propag.*, Vol. 49, No. 12, 1645–1648, 2001.
60. Ginzburg, V. L., *The Propagation of Electromagnetic Waves in Plasmas*, Pergamon Press, Oxford, 1970.
61. Felsen, L. B. and N. Marcuvitz, *Radiation and Scattering of Waves*, Prentice-Hall, Englewood Cliffs, 1973.
62. Lee, S. W. and Y. T. Lo, "Current distribution and input admittance of an infinite cylindrical antenna in anisotropic plasma," *IEEE Trans. Antennas Propag.*, Vol. 15, No. 2, 244–252, 1967.
63. Lee, S. W., "Cylindrical antenna in uniaxial resonant plasmas," *Radio Sci.*, Vol. 4, No. 2, 179–189, 1969.
64. Chugunov, Yu. V., "The theory of a thin metal antenna in anisotropic media," *Radiophys. Quantum Electron.*, Vol. 12, No. 6, 661–664, 1969.
65. Zaboronkova, T. M., A. V. Kudrin, and E. Yu. Petrov, "VLF current distribution on a cylindrical VLF antenna in a magnetoplasma," *Radiophys. Quantum Electron.*, Vol. 42, No. 8, 660–673, 1999.
66. Kudrin, A. V., E. Yu. Petrov, G. A. Kyriacou, and T. M. Zaboronkova, "Insulated cylindrical antenna in a cold magnetoplasma," *Progress In Electromagnetics Research*, Vol. 53, 135–166, 2005.
67. Gradshteyn, I. S. and I. M. Ryzhik, *Tables of Integrals, Series and Products*, Academic Press, New York, 2007.
68. Tamir, T. and A. A. Oliner, "The spectrum of electromagnetic waves guided by a plasma layer," *Proc. IEEE*, Vol. 51, No. 2, 317–332, 1963.
69. Shevchenko, V. V., *Continuous Transitions in Open Waveguides*, Golem Press, Boulder, 1971.